MRS Communications (2018), *8*, 1230–1235
© Materials Research Society, 2018
doi:10.1557/mrc.2018.111

MRS Communications

Research Letter

Electrocatalytic activity of high-entropy alloys toward oxygen evolution reaction

Xiaodan Cui, Boliang Zhang, Congyuan Zeng, and **Shengmin Guo,** Department of Mechanical & Industrial Engineering, Louisiana State University, Baton Rouge, Louisiana 70803, USA

Address all correspondence to Shengmin Guo at **sguo2@lsu.edu**

(Received 26 May 2018; accepted 15 June 2018)

Abstract

Due to the special crystal structures and electron configurations, high-entropy alloys (HEAs) are expected to have favorable activities for electrocatalytic reactions. In this paper, a set of oxygen evolution reaction (OER) criteria are applied for the HEA-based electrocatalyst design. Specifically, FeNiMnCrCu HEA is predicted to have a better OER performance than the baseline FeCoNiCrAl HEA. To demonstrate this design approach, both FeNiMnCrCu and FeCoNiCrAl samples are prepared and tested. Their crystal structures and electrocatalytic performance are examined. This paper demonstrates the potential of using finely tuned HEAs for OER applications.

Background

Due to the rapidly increasing demand for renewable and clean energy sources, water electrolysis has been examined frequently as a possible route for hydrogen generation.[1] However, owing to the common usage of high-cost noble metal-based electrocatalysts for oxygen evolution reaction (OER), such as Ir, Ru, and Pt, the large-scale industrialization of water electrolysis is impeded.[2] Recently, many low-cost materials have been explored to replace noble metals for OER.[3,4] Among them, first row transition metals, such as Ni, Fe, Co, Cu, and Mn, are especially appealing, due to their special electronic structures and the abundance on earth.[5] High-entropy alloys (HEAs), a new type of alloys, constructed of five or more metallic elements at equal or near-equal molecular ratios,[6,7] are emerging into an attractive category of functional metallic materials in the past decade.[8] Due to the varied atomic radius and geometrical configurations of different elements, the crystal lattices of HEAs can be finely tuned over a certain range, and the crystal lattices of HEAs can be severely distorted with significant residual strain remaining.[9] Such a high level of crystal imperfection could effectively increase the amount of active catalytic sites.[10] Moreover, due to the highly complex combination of transition metals with different electron configurations, the *d*-band vacancy number of HEA can be altered to tune its binding strength toward reaction species.[11] Because few studies have been conducted on the catalytic performance of HEAs, this paper examines the hypothesis that by tuning the HEAs compositions, an improved OER performance would be achieved.

HEA design for improved OER performance

The binding strength of the reaction species toward the surfaces of an electrocatalyst determines the activity of the electrocatalyst. For selected metallic catalysts, the volcano plot of catalytic activity versus the absorption energy of atomic oxygen[12] reveals that a moderate binding strength leads to a high catalytic activity. For OER applications, a weak binding between the reaction species and the electrocatalyst surface would result in difficult stabilization of intermediates, while a too strong binding would hinder the release of O_2. The binding strength is affected by several factors. Firstly, it is affected by the electronic structures of the electrocatalyst. The existence of *d*-band vacancy in transition metals enables the formation of intermediate species to lower the activation energy, and a moderate *d*-vacancy number is preferable for OER applications.[13] Secondly, in the heterogeneous reactions, the lattice spacing of the electrocatalyst and the reaction species should match. In other words, too large an interatomic distance would impede diatomic reactant adsorption and the bond formation between oxygen atoms, while too closely packed atoms would cause strong repulsions between intermediates and inhibit product formation.[13] Thirdly, a certain degree of intrinsic structural defects could contribute to an improved catalytic performance.[14] Therefore, compared with the traditional metals and alloys, a well-designed HEA with proper compositions is highly possible to combine the merits of each constitute element and meet the above criteria for improved OER performance.

Based on the criterion number 1, two HEAs were selected to demonstrate that HEA compositions would impact the OER performance. The first HEA would have a non-transition metal element and the second HEA would be formed by pure transition metals. In this regard, the classical FeCoNiCrAl HEA, with non-transition metal element Al, was chosen as the starting point to investigate how HEAs could be designed to have an improved OER performance. For FeCoNiCrAl

https://doi.org/10.1557/mrc.2018.111 Published online by Cambridge University Press

HEA, Fe, Co, Ni, and Cr are all on the left side of the peak on the volcano plot,[12] indicating their overstrong binding strength toward the reactant. Also, being a main group element, Al is a strong electron donor that can bind strongly to electron accepters to form stable compounds. All these may aggravate the difficulty of O_2 formation and release.

Based on the criterion number 2, the bond length of *M*–O (*M* = metal) for Fe, Co, Ni, Cr, and Al is 2.08, 2.13, 2.09, 2.02, and 1.89 Å, respectively[15–17] with an average of 2.04 Å. Considering the symmetric trapezoid configuration of OER diatomic reaction in the alkaline environment,[18] the calculated optimal lattice spacing to facilitate O_2 formation for a perfect electrocatalyst is ~2.50 Å. However, from the x-ray diffraction (XRD) testing results, to be shown in later section, FeCoNiCrAl mainly composes a FCC phase with $a = 3.3183 \pm 0.0013$ Å, demonstrating the lattice spacing for the most densely packed plane (111) to be 2.35 Å. Therefore, tuning the baseline FeCoNiCrAl HEA compositions with elements that can slightly decrease the *d*-vacancy number and enlarge the lattice spacing is expected to improve the activity of HEA electrocatalyst.

To design an HEA with more favorable features as an electrocatalyst toward OER, we decided to replace Co and Al with Mn and Cu. Because Cu has fully filled *d* orbitals, the electrons in Cu can transit to the *d*-band of other transition metals to reduce the *d*-vacancy number and the overall binding strength can be reduced. In addition, Mn ($r = 161$ pm) is among the few low-cost elements with an apparent larger radius than that of Al ($r = 118$ pm) and Co ($r = 152$ pm) and has an acceptable affinity toward O atom. With more matched *d*-vacancy number and lattice spacing toward OER, the FeNiMnCrCu HEA is expected to have a better performance than the baseline FeCoNiCrAl HEA.

Experimental

To synthesize the FeNiMnCrCu HEA, commercial iron (fine powder, Sigma Aldrich, St. Louis, MO, USA, >99%, metals basis), nickel (3–7 μm, Alfa Aesar, Ward Hill, MA, USA, >99.9%, metals basis), manganese (325 mesh, Alfa Aesar, 99.95%, metals basis), chromium (325 mesh, Alfa Aesar, 99%, metals basis), and copper (~170 + 400 mesh, Alfa Aesar, 99.5%, metals basis) powders with the ratio of 1:1:1:1:1 were well mixed inside a polystyrene ball mill jar by a high-speed ball milling machine for 2 min. Then the mixed powders were pressed in a dry pressing die with a diameter of 12.7 mm. Next, the as-prepared sample was placed into the chamber of an arc melting system (model Edmund Bühler/MAM-1). During the melting process, the ingots were inverted and re-melted for four times to ensure homogeneity. The FeCoNiCrAl HEA was prepared the same way by using equivalent mole amount of iron, cobalt (325 mesh, Alfa Aesar, 99.5%, metals basis), nickel, chromium, and aluminum (325 mesh, Alfa Aesar, 99.5%, metals basis).

The HEA phase diagrams are calculated by ThermoCalc™ software. The crystal structures of the HEA samples were characterized by XRD using a Rigaku MiniFlex diffractometer with Cu K_α radiation operated at 30 kV and 15 mA with a scan rate of 2°/min. The lattice parameters of each phase in the HEAs are calculated based on Bragg's law. Firstly, phases are identified according to the experimental results and the known compositions; then each peak in the spectra is indexed to *h*, *k*, *l* miller indices; next, the lattice spacing d_{hkl} is calculated according to the peak position; and finally, lattice parameters are derived statistically. To prepare the HEA electrode, a copper wire was attached to each of the arc-melted ingots by tin soldering. Then the ingots with the connecting wire were mounted into an epoxy resin (SamplKwick fast cure acrylic resin, Buehler, Lake Bluff, IL, USA). At last, for each sample, a flat surface was exposed by cutting through the ingot using a low-speed saw. The electrochemical measurements were carried out in a three-electrode system using a CHI 650C electrochemical workstation. The HEAs served as the working electrode in a 1 M NaOH aqueous electrolyte, with Pt wire and saturated calomel electrode (SCE) as counter electrode and reference electrode, respectively. Linear sweep voltammetry (LSV) and Tafel measurement were carried out at a scan rate of 5 mV/s in the potential range of 0–1 V versus SCE. Commercial Pt was tested the same way for comparison. Electrochemical impedance spectra (EIS) measurements were carried out at 438 mV overpotential in the frequency range from 10^5 to 0.01 Hz. To study the stability of the HEAs, the chronoamperometry was carried out at 438 mV overpotential for 10 h.

Results and discussion

CALPHAD method was adopted to calculate the phase diagram and the phase composition during an equilibrium solidification process. For the baseline quinary HEA system $FeCoNiCrAl_x$, with increasing of the Al content, the phase structure of the system gradually changes from a single FCC into a single BCC structure. This prediction has been proved experimentally by other researchers.[19] Figure 1(a) shows the pseudobinary phase diagram of FeCoNiCr-Al_x system calculated using ThermoCalc software. While keeping the molecular ratio of FeCoNiCr constant, the phase structure change, along with the (FeCoNiCr) and Al ratio, was presented as an ordinary binary phase diagram. Using the phase diagram, the equimolar $FeCoNiCrAl_{x=1}$ can be seen consisting of both FCC and BCC structures, with FCC phase as the primary phase. Under the sample preparation condition with a rapid cooling rate, equilibrium phase transformation at low temperatures is usually inhibited, leading to the precipitation of high-temperature phases.

Figure 1(b) shows the equilibrium solidification process of FeNiMnCrCu, starting from the liquidus temperature at ~1458 K. Both FCC and BCC phases start to form almost simultaneously, with a secondary FCC phase that forms at ~1297 K, which is almost the solidus temperature (1295 K). Considering the rapid cooling rate of the sample made in the water-cooled copper hearth of the arc melting furnace, the diffusion-introduced phase transformation at low temperatures could be neglected. Thus, the phase structures of FeNiMnCrCu should consist mainly of double FCC phases

https://doi.org/10.1557/mrc.2018.111 Published online by Cambridge University Press

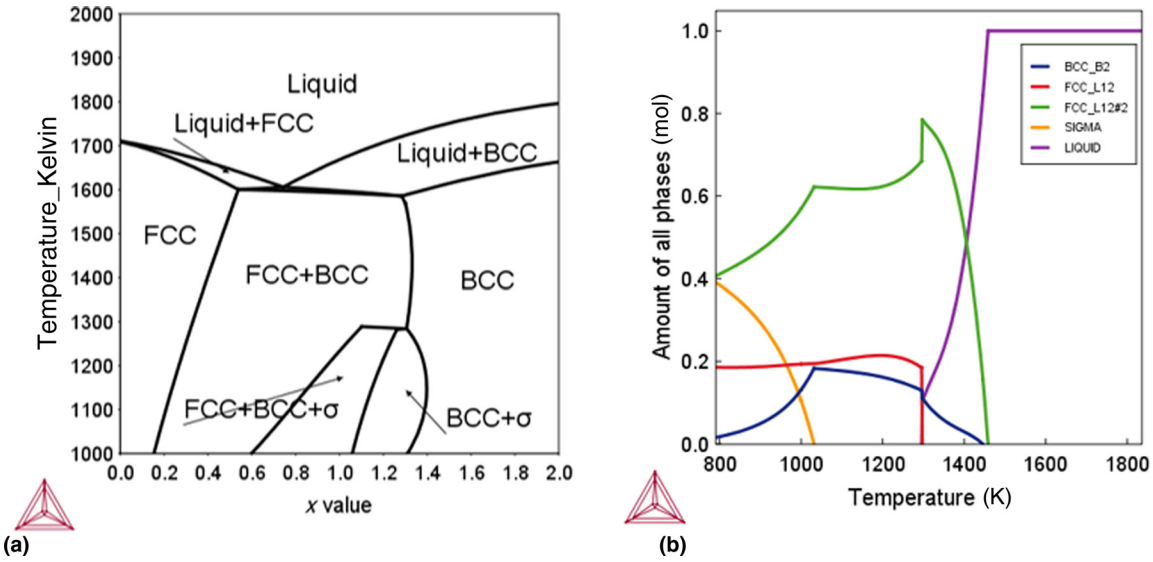


Figure 1. (a) Pseudobinary phase diagram of FeCoNiCr-Al$_x$; (b) phase composition during equilibrium solidification of FeNiMnCrCu.

and a BCC phase. It is also interesting to see that the intrinsic residual strain of FeNiMnCrCu is reported to be 3.18%[20] that is higher than the FeCoNiCrAl case value of 2.96%.[20] Therefore, the FeNiMnCrCu HEA is in a more non-equilibrium state possessing higher potential energy that is expected to activate reactions at a lower applied potential.[21]

The XRD patterns are presented in Fig. 2. The XRD spectrum of FeCoNiCrAl indicates a complete dissolution of all five elements and the formation of a single FCC phase. This differs from the equilibrium prediction shown in Fig. 1(a). Based on other researchers, FCC is the major structure of the FeCoNiCrAl HEA annealed at a temperature higher than 800°C and then free cooled to room temperature.[22] Under the arc melting process, the rapid cooling rate inhibits phase transformation to BCC and leads to the domination of the FCC phase. Peaks at $2\theta = 43.85°$, 51.08°, 75.09° 91.34°, and 96.59° corresponding to the planes of (111), (200), (220), (311), and (222) of the FCC can be observed. The lattice parameter is calculated to be $a = 3.3183 \pm 0.0013$ Å.

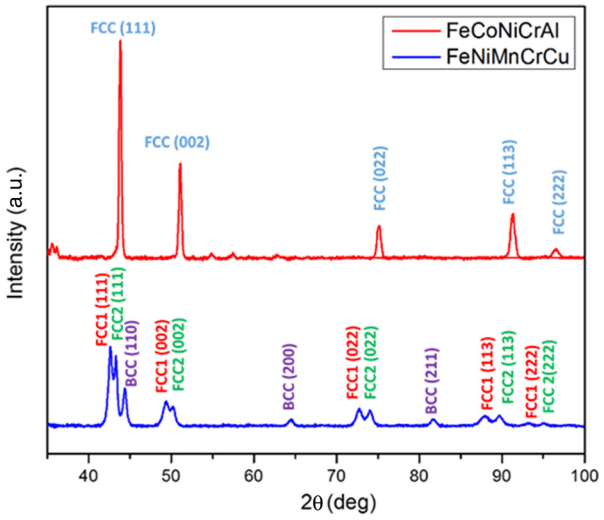


Figure 2. XRD spectra of FeCoNiCrAl and FeNiMnCrCu.

For the FeNiMnCrCu HEA, it has a more complicated structure and is composed of two FCC and one BCC phases. The first FCC phase has peaks at $2\theta = 42.59°$, 49.40°, 72.78°, 87.89°, and 93.34° corresponding to the planes of (111), (200), (220), (311), and (222). The lattice parameter is calculated to be $a = 3.4160 \pm 0.0055$ Å. The second FCC phase has peaks at $2\theta = 43.43°$, 50.24°, 74.05°, 89.77°, and 95.02° corresponding to the planes of (111), (200), (220), (311), and (222). The lattice parameter is calculated to be $a = 3.3601 \pm 0.0076$ Å. The BCC phase has peaks at $2\theta = 44.38°$, 64.51°, and 81.81° corresponding to the planes of (110), (200), and (211). The lattice parameter is calculated to be $a = 2.678 \pm 0.0020$ Å. Therefore, the lattice constants of the FCC phases in the FeNiMnCrCu are larger than that of FeCoNiCrAl. This is due to the replacement of Al ($r = 118$ pm) and Co ($r = 152$ pm) by Cu (145 pm) and Mn (161 pm), whose radii are relatively larger, causing the extension of lattice. In addition, due to the higher atomic packing density of FCC (74%) than that of BCC (68%), the replacing of Al and Co with Cu and Mn leads to a mixture of FCC and BCC phases and causes larger residual strains. This gives higher lattice distortion energy. Therefore, to release the distortion energy, some of the FCC phase splits to two different FCC phases, with the rest transfers to a more stable BCC phase.[23] It can be seen that the lattice spacing of {111} planes in FCC1 and FCC2 phases of FeNiMnCrCu HEA are 2.38 and 2.42 Å, respectively, which are closer to the optimal lattice spacing (2.50 Å) than that of FeCoNiCrAl HEA (2.35 Å).

https://doi.org/10.1557/mrc.2018.111 Published online by Cambridge University Press

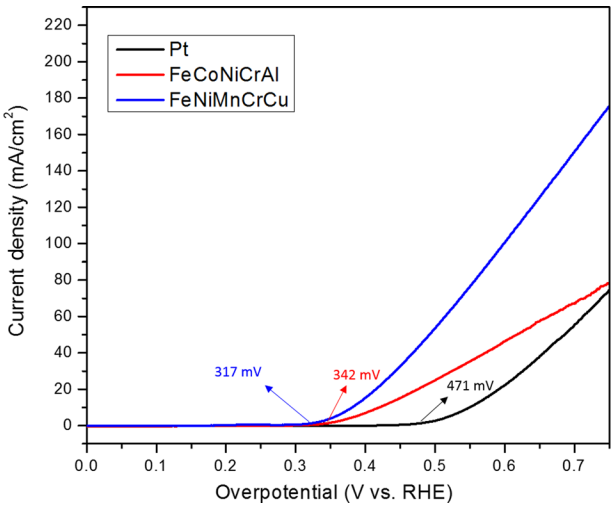


Figure 3. The OER polarization curves of FeCoNiCrAl and FeNiMnCrCu electrodes.

To evaluate the electrocatalytic performance of FeCoNiCrAl and FeNiMnCrCu HEAs, the LSV results are shown in Fig. 3. Onset overpotential is the overpotential where the OER current starts to generate, defined by the point where the current density starts to sharply increase on the LSV spectra as labeled on Fig. 3. It is seen that the onset overpotentials for FeCoNiCrAl and FeNiMnCrCu HEAs are 317 and 342 mV, respectively, which are significantly lower than that of the Pt electrode (471 mV), indicating a lower activation energy needed by the HEA electrocatalysts to initialize the OER redox reaction.[24] The FeCoNiCrAl electrode exhibits a relatively lower activity with slowly increased current density and is not able to reach an OER current density of 100 mA/cm^2 in the tested voltage range. It is observed that the FeNiMnCrCu electrode possesses a better electrocatalytic activity with the current density increasing rapidly after the onset potential and reaches 40 and 100 mA/cm^2 OER current density at 466 and 599 mV overpotential, respectively. For comparison, FeCoNiCrAl and Pt electrodes require 580 and 656 mV to achieve 40 mA/cm^2, respectively. It can be seen that HEAs have a great potential in serving as OER electrocatalyst due to their much improved performance than the Pt electrocatalyst. In addition, as expected, the performance of the FeNiMnCrCu HEA electrocatalyst is significantly higher than that of FeCoNiCrAl, due to its higher residual strain, better matched *d*-vacancy number and lattice spacing toward OER.

To study the kinetic of the OER with HEA electrocatalysts, the Tafel plots are provided in Fig. 4(a). In the Tafel plots, a smaller slope indicates a more rapid electron transfer at the electrode and electrolyte interface at the applied potentials, suggesting a better catalytic activity of the electrocatalyst.[25] Tafel slopes for FeCoNiCrAl, FeNiMnCrCu, and Pt electrodes are 75, 58, and 66 mV/decade, respectively. It can be seen that the Tafel slope of FeNiMnCrCu is smaller than Pt. The electrochemical process is further studied by EIS at an overpotential of 438 mV in the frequency range of 10^5–0.01 Hz as displayed in Fig. 4(b). The equivalent circuit elements are fitted by CHI 650 C electrochemical workstation software package with the results listed in Table I. The intercept of the plot with the horizontal axis at high frequency (R_s) is the overall series resistance, including material bulk resistance and contact resistance.[26,27] The first semicircle with a diameter of R_{int} is due to the metal hydroxide intermediates formation.[28] It is noticed that the R_{int} of FeNiMnCrCu (0.065 Ω cm^2) is apparently lower than that of FeCoNiCrAl (0.177 Ω cm^2), demonstrating a more facilitated OH^- absorption and intermediate formation at the electrode and electrolyte interface, which could effectively lower down the activation energy of the electrochemical reaction. It is also noticed that the CPE_1 of FeNiMnCrCu (1.393 mF s^{n-1} cm^{-2}) is larger than that of FeCoNiCrAl (0.650 mF s^{n-1} cm^{-2}), indicating more atoms on FeNiMnCrCu surface are involved in reaction species absorption, attributed to its more distorted crystal structure. The second semicircle describes the electron charge transportation process of the OER redox reaction, with a diameter of R_{ct}

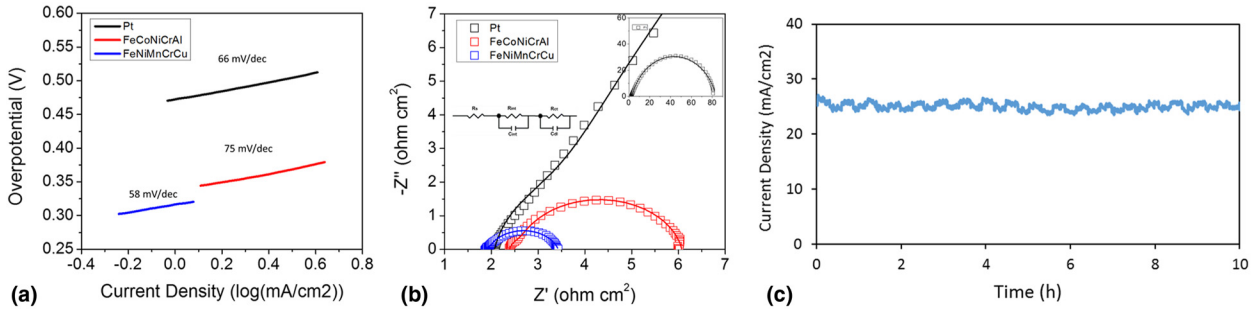


Figure 4. (a) Tafel slopes of FeCoNiCrAl and FeNiMnCrCu electrodes and (b) the EIS spectra of FeCoNiCrAl and FeNiMnCrCu electrodes; symbols: experimental data; solid lines: simulated data; inset: equivalent circuit; (c) time-dependent potential response during 10 h chronoamperometric water-splitting reaction, at a constant DC potential of 438 mV overpotential.

https://doi.org/10.1557/mrc.2018.111 Published online by Cambridge University Press

Table I. EIS parameters.

Sample	R_s (Ω cm^2)	R_{int} (Ω cm^2)	CPE$_1$ (mF s^{n-1} cm^{-2})	n_1	R_{ct} (Ω cm^2)	CPE$_2$ (mF s^{n-1} cm^{-2})	n_2
FeCoNiCrAl	2.393	0.177	0.650	0.999	3.505	1.764	0.891
FeNiMnCrCu	1.882	0.065	1.393	0.999	1.482	9.516	0.820
Pt	2.065	0.995	0.295	0.999	80.627	0.865	0.825

representing the charge transfer resistance.[28] It can be seen that the R_{ct} of FeNiMnCrCu (1.482 Ω cm^2) is much smaller than that of FeCoNiCrAl electrode (3.505 Ω cm^2), indicating a faster electron transfer rate from reactant to product. As it is observed, the superior electrochemical characteristic of FeNiMnCrCu is the result of its optimized binding strength toward reaction species. A better matched *d*-vacancy number effectively accelerates electron transfers and the matched lattice spacing facilitates the reactant absorption and product desorption, and the high residual strain contributes to a higher potential energy that can activate OER at a lower overpotential. The stability of the FeNiMnCrCu HEA electrocatalyst was evaluated by the chronoamperometry at a potential of 438 mV overpotential for 10 h [Fig. 4(c)]. The FeNiMnCrCu HEA displays an initial current density of ~26 mA/cm^2 and maintains this performance without significant changes for 10 h, which indicates a good electrochemical reversibility in the extensive OER durability testing.

It can be seen that compared with traditional metals and alloys, a well-designed HEA can combine the merits of each constitute element and become an efficient electrocatalyst toward OER. Firstly, since the atomic structure in HEAs is highly complex with random occupancies of elements in the lattice, the crystal structure of a HEA can be highly distorted with non-negligible residual strain. As a result, the atoms are in a thermodynamically metastable state possessing higher potential energy and more catalytic active sites. It is noticed that the lattice distortion in FeNiMnCrCu is more severe that leads to its higher catalytic activity than FeCoNiCrAl. Secondly, due to the combination of different elements, the atomic lattice spacing and electronic configuration can be tuned to match better with OER.

Conclusions

Due to the unique crystal structures with severe lattice distortions, HEA-based electrocatalysts may possess attractive electrocatalytic properties. In this study, based on a set of OER criteria, two transition metal-based HEAs, namely FeNiMnCrCu and FeCoNiCrAl, are selected to demonstrate that the compositions of HEAs could be tuned to improve the OER performance. Both FeNiMnCrCu and FeCoNiCrAl samples are prepared and tested. Their crystal structures and electrocatalytic performance are examined. Owing to the replacement of Al and Co by Cu and Mn, the *d*-vacancy number and lattice spacing for FeNiMnCrCu are more suitable for improved OER performances. In comparison with the baseline FeCoNiCrAl and the platinum, FeNiMnCrCu needs less activation energy to initialize the OER reactions and its current density increases more rapidly with a potential than that of FeCoNiCrAl and platinum. As predicted, FeNiMnCrCu exhibits a good activity toward OER, which demonstrates the potential of using finely tuned HEAs for electrocatalytic applications.

Acknowledgments

This publication is based upon the work supported by NSF-Consortium for innovation in manufacturing and materials (CIMM) program (grant number # OIA-1541079).

References

1. D.L. Stojić, M.P. Marčeta, S.P. Sovilj, and Š.S. Miljanić: Hydrogen generation from water electrolysis—possibilities of energy saving. *J. Power Sources* **118**, 315 (2003).
2. Y. Lee, J. Suntivich, K.J. May, E.E. Perry, and Y. Shao-Horn: Synthesis and activities of rutile IrO2 and RuO2 nanoparticles for oxygen evolution in acid and alkaline solutions. *J. Phys. Chem. Lett.* **3**, 399 (2012).
3. M.S. Faber and S. Jin: Earth-abundant inorganic electrocatalysts and their nanostructures for energy conversion applications. *Energy Environ. Sci.* **7**, 3519 (2014).
4. A. Liu, Z. Chen, X. Wei, W. Xiao, and J. Ding: Economical Fe-doped Ta2O5 electrocatalyst toward efficient oxygen evolution: a combined experimental and first-principles study. *MRS Commun.* **7**, 563 (2017).
5. L. Fei, Z. Min, Z. Yuxue, and Z. Xianghua: First-row transition metal based catalysts for the oxygen evolution reaction under alkaline conditions: basic principles and recent advances. *Small* **13**, 1701931 (2017).
6. B. Zhang, Y. Mu, M.C. Gao, W.J. Meng, and S.M. Guo: On single-phase status and segregation of an as-solidified septenary refractory high entropy alloy. *MRS Commun.* **7**, 78 (2017).
7. J. Wang, Y. Zhang, S.Z. Niu, W.Y. Wang, H.C. Kou, J.S. Li, S.Q. Wang, and E. Beaugnon: Formation of a hexagonal closed-packed phase in Al0.5CoCrFeNi high entropy alloy. *MRS Commun.* **7**, 879 (2017).
8. D.B. Miracle and O.N. Senkov: A critical review of high entropy alloys and related concepts. *Acta Mater.* **122**, 448 (2017).
9. Z. Wang, W. Qiu, Y. Yang, and C.T. Liu: Atomic-size and lattice-distortion effects in newly developed high-entropy alloys with multiple principal elements. *Intermetallics* **64**, 63 (2015).
10. T. Bak, J. Nowotny, N.J. Sucher, and E. Wachsman: Effect of crystal imperfections on reactivity and photoreactivity of TiO2 (rutile) with oxygen, water, and bacteria. *J. Phys. Chem. C* **115**, 15711 (2011).
11. Z.Y. Lv, X.J. Liu, B. Jia, H. Wang, Y. Wu, and Z.P. Lu: Development of a novel high-entropy alloy with eminent efficiency of degrading azo dye solutions. *Sci. Rep.* **6**, 34213 (2016).
12. J.K. Nørskov, J. Rossmeisl, A. Logadottir, L. Lindqvist, J.R. Kitchin, T. Bligaard, and H. Jónsson: Origin of the overpotential for oxygen reduction at a fuel-cell cathode. *J. Phys. Chem. B* **108**, 17886 (2004).
13. J.M. Thomas and J.W. Thomas (Eds). *Principles and Practice of Heterogeneous Catalysis*. 2nd ed. 2015. ISBN: 978-3-527-31458-4.

https://doi.org/10.1557/mrc.2018.111 Published online by Cambridge University Press

14. X. Cui, W. Xu, Z. Xie, J.A. Dorman, M.T. Gutierrez-Wing, and Y. Wang: Effect of dopant concentration on visible light driven photocatalytic activity of Sn1-xAgxS2. *Dalton Trans.* **45**, 16290 (2016).
15. I.D. Brown and R.D. Shannon: Empirical bond-strength–bond-length curves for oxides. *Acta Crystallogr. Sect. A* **29**, 266 (1973).
16. J.A. Mejias, V. Staemmler, and H.J. Freund: Electronic states of the Cr 2 O 3 (0001) surface from ab initio embedded cluster calculations. *J. Phys. Condens. Matter* **11**, 7881 (1999).
17. L.S. Caputi, S.L. Jiang, A. Amoddeo, and R. Tucci: Oxygen-nickel bond length in Ni(111)-O determined by electron-energy-loss fine-structure spectroscopy. *Phys. Rev. B* **41**, 8513 (1990).
18. X. Cui, B. Zhang, C. Zeng, H. Wen, H. Yao, and S. Guo: Laser processed Ni-Fe alloys as electrocatalyst toward oxygen evolution reaction. *Mater. Res. Express* **5**, 066527 (2018).
19. H.-P. Chou, Y.-S. Chang, S.-K. Chen, and J.-W. Yeh: Microstructure, thermophysical and electrical properties in AlxCoCrFeNi ($0 \leq x \leq 2$) high-entropy alloys. *Mater. Sci. Eng. B* **163**, 184 (2009).
20. Y.F. Ye, C.T. Liu, and Y. Yang: A geometric model for intrinsic residual strain and phase stability in high entropy alloys. *Prog. Mater. Sci.* **94**, 152 (2015).
21. T. Egami: Atomic level stresses. *Prog. Mater. Sci.* **56**, 637 (2011).
22. W. Ji, Z. Fu, W. Wang, H. Wang, J. Zhang, Y. Wang, and F. Zhang: Mechanical alloying synthesis and spark plasma sintering consolidation of CoCrFeNiAl high-entropy alloy. *J. Alloys Compd.* **589**, 61 (2014).
23. K.B. Zhang, Z.Y. Fu, J.Y. Zhang, W.M. Wang, H. Wang, Y.C. Wang, Q. J. Zhang, and J. Shi: Microstructure and mechanical properties of CoCrFeNiTiAlx high-entropy alloys. *Mater. Sci. Eng. A* **508**, 214 (2009).
24. T. Zhou, Z. Cao, P. Zhang, H. Ma, Z. Gao, H. Wang, Y. Lu, J. He, and Y. Zhao: Transition metal ions regulated oxygen evolution reaction performance of Ni-based hydroxides hierarchical nanoarrays. *Sci. Rep.* **7**, 46154 (2017).
25. E. Fabbri, A. Habereder, K. Waltar, R. Kotz, and T.J. Schmidt: Developments and perspectives of oxide-based catalysts for the oxygen evolution reaction. *Catal. Sci. Technol.* **4**, 3800 (2014).
26. X. Cui, W. Xu, Z. Xie, and Y. Wang: High-performance dye-sensitized solar cells based on Ag-doped SnS2 counter electrodes. *J. Mater. Chem. A* **4**, 1908 (2016).
27. X. Cui, Z. Xie, and Y. Wang: Novel CoS2 embedded carbon nanocages by direct sulfurizing metal-organic frameworks for dye-sensitized solar cells. *Nanoscale* **8**, 11984 (2016).
28. D.V. Franco, L.M. Da Silva, W.F. Jardim, and J.F.C. Boodts: Influence of the electrolyte composition on the kinetics of the oxygen evolution reaction and ozone production processes. *J. Braz. Chem. Soc.* **17**, 746 (2006).

https://doi.org/10.1557/mrc.2018.111 Published online by Cambridge University Press